MULTIBENCH++: A Unified and Comprehensive Multimodal Fusion Benchmarking Across Specialized Domains

Leyan Xue¹, Changqing Zhang^{1*}, Kecheng Xue², Xiaohong Liu³, Guangyu Wang², Zongbo Han^{2*}

¹College of Intelligence and Computing, Tianjin University, Tianjin, China

²State Key Laboratory of Networking and Switching Technology, Beijing University of Posts and Telecommunications, Beijing, China

³Institute of Medical Artificial Intelligence, South China Hospital, Medical School, Shenzhen University, Guangdong, China

Abstract

Although multimodal fusion has made significant progress, its advancement is severely hindered by the lack of adequate evaluation benchmarks. Current fusion methods are typically evaluated on a small selection of public datasets, a limited scope that inadequately represents the complexity and diversity of real-world scenarios, potentially leading to biased evaluations. This issue presents a twofold challenge. On one hand, models may overfit to the biases of specific datasets, hindering their generalization to broader practical applications. On the other hand, the absence of a unified evaluation standard makes fair and objective comparisons between different fusion methods difficult. Consequently, a truly universal and high-performance fusion model has yet to emerge. To address these challenges, we have developed a largescale, domain-adaptive benchmark for multimodal evaluation. This benchmark integrates over 30 datasets, encompassing 15 modalities and 20 predictive tasks across key application domains. To complement this, we have also developed an open-source, unified, and automated evaluation pipeline that includes standardized implementations of state-of-the-art models and diverse fusion paradigms. Leveraging this platform, we have conducted large-scale experiments, successfully establishing new performance baselines across multiple tasks. This work provides the academic community with a crucial platform for rigorous and reproducible assessment of multimodal models, aiming to propel the field of multimodal artificial intelligence to new heights.

Code — https://github.com/ravexly/MultiBenchplus

1 Introduction

Multimodal data, such as text, images, and sensor signals, is driving the next generation of artificial intelligence. Through a technique known as Multimodal Fusion, AI systems can integrate and understand information from these diverse sources, achieving a more comprehensive, accurate, and robust understanding than is possible with any single source (Baltrušaitis, Ahuja, and Morency 2018; Xu, Zhu, and Clifton 2023). This capability is a key driver for advancing AI to higher levels of intelligence and shows immense

Copyright © 2026, Association for the Advancement of Artificial Intelligence (www.aaai.org). All rights reserved.

potential in fields like autonomous driving and medical diagnostics (Caesar et al. 2020; Azam et al. 2022).

However, a significant divergence exists between multimodal research and other domains. While fields such as natural language processing and graph learning have successfully converged on dominant architectural paradigms, specifically the Transformer and GNNs, the multimodal domain conspicuously lacks an equivalent unified, foundational framework. Progress remains highly fragmented; researchers typically validate new methods on a small, bespoke selection of classic datasets. This reliance on siloed benchmarks is a key bottleneck. It not only leads to models overfitting to specific data biases and prevents fair objective comparisons, but more importantly, it has hindered the systematic search for a truly general-purpose fusion architecture. Four years ago, the groundbreaking MULTIBENCH framework partially addressed this by providing a unified evaluation platform. Yet, with the field's rapid evolution, its limitations are now apparent, and it is no longer sufficient to meet today's challenges.

The urgent need for a new foundational platform stems from two primary trends. The first is the explosive growth in data combinatorial complexity. Unlike unimodal tasks, realworld applications in medical imaging, IoT, and autonomous driving (Hu et al. 2023; Kong et al. 2011) span a vast, heterogeneous spectrum. This combinatorial effect, where different data combinations can yield entirely different analytical conclusions, means older, simpler benchmarks can no longer demonstrate a model's robustness or adaptability to realworld complexity. The second trend is the rapid evolution of fusion models, especially Transformer-based methods (Wei et al. 2020; Wang et al. 2022; Xu, Zhu, and Clifton 2023). Without a standardized, complex testbed, it is impossible to determine if these new models are truly general-purpose or simply adept at specific data combinations. Therefore, a platform that forces models to confront this combinatorial complexity has become essential to guide the search for a foundational architecture.

To address key challenges in evaluating next-generation multimodal fusion models, we introduce MULTI-BENCH++, a new, large-scale benchmark. Instead of being a simple incremental update, MULTIBENCH++ represents a significant leap forward in terms of scale, domain diversity, and suitability for modern architectures.

^{*}Corresponding author.

Table 1: MULTIBENCH++ offers a unified benchmark suite of 37 multimodal datasets spanning a wide spectrum of research fields, data scales, input modalities(a: audio, c: clinical/tabular, d: depth/DSM, e: events/spiking, f: 2D fundus, g: GIS, h: HSI, i: image, k: time-series, L: LiDAR, m: multispectral, M: metadata, o: multi-omics, O: 3D OCT, s: SAR, t: text, v: video, with omics sub-typed as o_1 : mRNA, o_2 : miRNA, o_3 : DNA), and downstream tasks.

Domain	Dataset	Modalities	# Samples	Prediction Task
	Houston2013	$\{h, L\}$	14,999	Land Cover Classification
	Houston2018	$\{h, L\}$	2,018,910	Land Cover Classification
Domoto Consina	MUUFL Gulfport	$\{h, L\}$	53,687	Land Cover Classification
Remote Sensing	Trento	$\{h, L\}$	30,214	Land Cover Classification
	Berlin	$\{h,s\}$	464,671	Land Cover Classification
	MDAS (Augsburg)	$\{h,s\}$	78,294	Land Cover Classification
	ForestNet	$\{c,i,m\}$	2,757	Forest Type Mapping
	TCGA-BRCA	$\{o_1, o_2, o_3\}$	875	Survival Prediction, Subtype Classification
	ROSMAP	$\{o_1, o_2, o_3\}$	351	Disease Progression Prediction
	SIIM-ISIC	$\{i,M\}$	33,126	Malignant Tumor Classification
Medical AI	Derm7pt	$\{i,M\}$	1,011	Lesion Diagnosis Prediction
Micuical Al	GAMMA	$\{f,O\}$	100	Glaucoma Grading
	MIMIC-III	$\{c,t\}$	36,212	Mortality Prediction
	MIMIC-CXR	$\{c,t\}$	372,147	Mortality Prediction, Multilabel Classification
	eICU	$\{c,t\}$	7,637	Mortality Prediction
	TCGA	$\{o_1, o_2, o_3\}$	306	Subtype classification, Tumor Malignancy Grading
	MELD	$\{a,t\}$	13,708	Emotion/Sentiment Recognition
	IEMOCAP	$\{a,v,t\}$	7,433	Emotion/Sentiment Recognition
	MAMI	$\{i,t\}$	11,000	Misogyny Content Detection
	Memotion	$\{i,t\}$	6,831	Offensive Content Detection
Affective Computing	MUTE	$\{i,t\}$	4,156	Hate Speech Detection
&Social Media	MultiOFF	$\{i,t\}$	743	Offensive Content Detection
Understanding	MET-Meme(C)	$\{i,t\}$	2,299	Metaphor/Emotion/Intent Recognition
Onderstanding	MET-Meme(E)	$\{i,t\}$	1,053	Metaphor/Emotion/Intent Recognition
	CH-SIMS	$\{a,v,t\}$	2,281	Sentiment Analysis
	CH-SIMS v2.0	$\{a,v,t\}$	4,403	Sentiment Analysis
	Twitter2015	$\{i,t\}$	5,338	Multimodal Named Entity Recognition
	Twitter1517	$\{i,t\}$	4,672	Multimodal Named Entity Recognition
	MIRFLICKR	$\{i,t\}$	20,015	Image Retrieval
	CUB Image-Caption	$\{i,t\}$	117,880	Fine-grained Classification
	SUN-RGBD	$\{i,d\}$	9,504	Scene Understanding, Object Detection
	NYUDv2	$\{i,d\}$	1,863	Scene Understanding, Object Detection
Others	UPMC-Food101	$\{i,t\}$	90,686	Food Recognition
	MVSA-Single	$\{i,t\}$	2,592	Sentiment Analysis
	MNIST-SVHN	$\{i,i\}$	660,680	Digit Recognition
	N-MNIST+N-TIDIGITS	$\{e,i\}$	4,050	Digit Recognition
	E-MNIST+EEG	$\{i,k\}$	702	Digit Recognition

Its core contributions are threefold:

- Expanded scale and domain coverage. MULTI-BENCH++ brings together over 30 datasets, more than doubling the size of its predecessor. More importantly, it extends into highly complex and specialized domains, including Remote Sensing, Healthcare, Affective Computing, and Social Media Analysis. These domains present unique data fusion challenges.
- Designed for rigorous testing of advanced architectures. Its datasets are carefully chosen for their high complexity, rich interplay between modalities, and naturally occurring missing data, creating a challenging test environment. This design allows for rigorous testing of advanced, Transformer-based architectures and novel fusion techniques.

• An open-source framework for robust and reproducible evaluation. To ensure fair and rigorous scientific comparisons, MULTIBENCH++ includes a standardized, opensource evaluation framework. This framework provides standardized data splits, Robustness Probes, and a set of strong baseline models that have been carefully tuned using Automated Hyperparameter Optimization. This infrastructure is designed to lower the barrier to entry for researchers and ensure that future innovations can be reliably evaluated on a fair and consistent foundation.

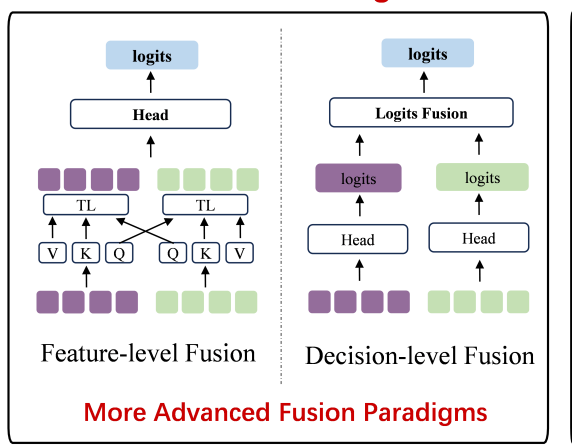
2 Related Works

Comparisons with Related Benchmarks. Multimodal research has been driven by a series of influential benchmarks. Foundational datasets for visual question answer-

Datasets

Specialized Domains 15+ Modalities Affective Text Image Health care computing He is a smart guy Table Audio SUBJECT ID Age Sex Ethnicity Remote Others sensing Video Time-series **ACMININGS** Me Note 1 **Broader & Deeper Datasets**

Fusion Paradigms



Tuning

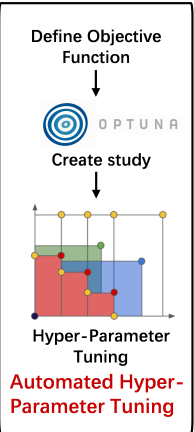


Figure 1: An overview of the MULTIBENCH++ framework, highlighting our core contributions. (Left) We introduce a broader and deeper collection of datasets, significantly expanding into more specialized domains and data modalities. (Center) We integrate more advanced fusion paradigms, including feature-level transformer-based fusion and decision-level fusion. (Right) We provide an automated hyper-parameter tuning platform, powered by Optuna, to ensure robust and reproducible evaluation.

ing, such as VQA-v2 (Goyal et al. 2017), established large-scale, open-ended visual reasoning as a core challenge. In parallel, benchmarks for multimodal sentiment analysis and emotion recognition, like CMU-MOSI (Zadeh et al. 2016) and the larger CMU-MOSEI (Zadeh et al. 2018), provided key testbeds for integrating language, visual, and acoustic signals. To standardize evaluation across this growing land-scape, frameworks like MULTIBENCH (Liang et al. 2021) were introduced to offer a unified, reproducible testbed for assessing model robustness across a diverse set of tasks. Building on this principle, our work expands this suite with 20 additional datasets, contributing to a broader trend of comprehensive evaluation that also includes integrating more competitive methods and developing automated tuning platforms.

Other works introduce new domains, such as MM-GRAPH (Zhu et al. 2025), which integrates visual features into graph-based tasks, and Dyn-VQA (Li et al. 2024), which tests dynamic question answering requiring multi-hop retrieval.

Multimodal Fusion. The core challenge in multimodal learning is fusion: the effective combination of information from different modalities. Classical approaches are categorized by the architectural stage at which fusion occurs: early (feature-level) fusion concatenates raw or low-level features (Ramachandram and Taylor 2017; Atrey et al. 2010), while late (decision-level) fusion combines outputs from modality-specific models (Soleymani et al. 2017; Han et al. 2022; Zhang et al. 2023). The advent of the Transformer has made attention-based fusion the dominant paradigm (Xu, Zhu, and Clifton 2023). These methods can be broadly classified as single-stream, where multimodal inputs are concatenated and processed by a unified encoder, or multi-stream, which uses separate encoders for each modality followed by cross-attention mechanisms to integrate information (Na-

grani et al. 2021). Such architectures allow for nuanced, dynamically-weighted integration of modal features. More recent research also focuses on developing fusion techniques that are robust to real-world challenges like noisy, incomplete, or imbalanced data (Zhang et al. 2024).

Analysis of Multimodal Representations. Beyond predictive performance, understanding the quality of learned multimodal representations is a critical area of research (Frome et al. 2013; Kiros, Salakhutdinov, and Zemel 2014). A primary technique is the use of probing tasks, where simple classifiers are trained on a model's internal embeddings to test for specific encoded properties (Alain and Bengio 2016). For example, studies have shown that global semantics are often encoded in the intermediate layers of MLLMs, while local, fine-grained details are captured in the final layers (Tao et al. 2024). Other works focus on interpretability and explainability, using techniques like visualizing attention maps or model dissection tools to attribute a model's decision to specific unimodal features (Liang, Zadeh, and Morency 2024). The overarching goal of these analysis is to measure fundamental properties like modality alignment, complementarity, and redundancy, which is crucial for building more robust and efficient models.

3 MULTIBENCH++ : A Broader & Deeper Multimodal Benchmark

3.1 Background

Multimodal datasets differ in both the types of information they provide and the ways that information is encoded. Remote sensing archives couple spectral bands with LiDAR point clouds, while electronic health records weave freetext notes together with structured lab values and pathology slides. Affective repositories, in turn, align video frames to audio streams and wearable signals. These collections

Algorithm 1 End-to-End Workflow with Optuna.

```
# 1. Load data and define models
   train_loader, val_loader, test_loader, n_classes = get_loader()
   encoders = [Modality1Encoder(args), Modality2Encoder(args)]
   fusion = TMC(n_classes)
5
   head = get_head(n_classes, decision=True)
   # 2. Define a minimal objective function
7
   def objective(trial):
8
       # Suggest hyperparameters
9
       params = {'lr': trial.suggest_loguniform('lr', 1e-5, 1e-3), ...}
10
       # Train a model and return its validation accuracy
11
       val_accuracy = train(encoders, fusion, head, params, ...)
12
       return val_accuracy
13
   # 3. Run the hyperparameter search
14
   study = optuna.create_study(direction='maximize')
   study.optimize(objective, n_trials=10)
   # 4. Get the best parameters and build the final model
17
   final_model = build_model(study.best_trial.number)
   # 5. Evaluate the final, optimized model
18
   test_accuracy = test(final_model, test_loader)
```

are rarely designed for joint use, so their formats, resolutions, and noise levels diverge. A benchmark must therefore expose models to this heterogeneity. As shown in Fig. 1, MULTIBENCH++ addresses the current evaluation gap by collecting over thirty datasets drawn from highly specialized domains including remote sensing, healthcare, affective computing and social media. These specialized domains are not arbitrary, they represent critical frontiers where multimodal integration is pivotal for scientific and societal progress. The inclusion of such a wide array of data sources ensures that the benchmark rigorously tests a model's ability to generalize across fundamentally different data structures and noise profiles, moving beyond single-domain evaluations.

3.2 Datasets

Remote Sensing for Environmental Intelligence The remote-sensing domain for environmental intelligence tackles land-cover classification, target detection, spectral unmixing, and related tasks by fusing data whose physical origins differ fundamentally. Optical and hyperspectral systems capture surface chemistry yet remain weatherdependent; SAR measures microwave backscatter day-andnight; LiDAR delivers centimetre-level topography and canopy structure. Integrating these streams requires reconciling disparate spatial resolutions, geometries, and noise statistics. Foundational datasets establish this task-oriented landscape. Houston2013 and Houston2018 (Debes et al. 2014; Xu et al. 2018) combine hyperspectral imagery with LiDAR for urban land-cover classification. MUUFL Gulfport (Gader et al. 2013) adds co-registered hyperspectral and LiDAR data over a university campus for classification and rare-target detection. Trento (University of Trento 2022) provides a rural counterpart with hyperspectral and LiDAR. Berlin (Okujeni, van der Linden, and Hostert 2016) fuses PolSAR and hyperspectral data, while ForestNet (Irvin et al. 2020) couples satellite imagery and airborne LiDAR for forest-type and biomass mapping. The recent MDAS

dataset (Hu et al. 2023) enriches the benchmark suite with simultaneous SAR, multispectral, hyperspectral, DSM, and GIS layers, supporting resolution enhancement, unmixing, and classification. Together, these datasets constitute a systematic test-bed for advancing theoretically grounded and practically robust environmental-intelligence algorithms.

Medical AI for Diagnostics and Prognosis The medicalintelligence domain addresses survival prediction, malignancy classification, disease-progression modelling and related tasks by fusing exceptionally heterogeneous data streams. Gigapixel whole-slide images quantify tissue morphology; high-dimensional omics profiles capture molecular aberrations; dense time-series vital signs and concise clinical narratives encode patient trajectories. Integrating these modalities demands reconciling extreme differences in resolution, scale and noise, while preserving clinical interpretability. Benchmark datasets anchor this landscape. TCGA-BRCA (Weinstein et al. 2013) couples WSIs with multi-omics for breast-cancer survival and subtype analysis. ROSMAP (Bennett et al. 2018) supplies longitudinal multi-omics and pathology to chart Alzheimer progression. In dermatology, SIIM-ISIC (Rotemberg et al. 2021) and Derm7pt (Kawahara et al. 2018) pair dermoscopic images with patient metadata for melanoma detection. GAMMA (Wu et al. 2023) fuses 2D fundus photographs with 3D OCT volumes for glaucoma grading and optic-disc/cup segmentation. MIMIC-III (Johnson et al. 2016), MIMIC-CXR (Johnson et al. 2019) and eICU (Pollard et al. 2018) deliver largescale ICU time series merged with static clinical records to support mortality prediction and disease-code classification.

Affective Computing and Social Media Understanding The Affective Computing domain addresses emotion recognition, sarcasm detection, sentiment analysis and related high-level tasks by fusing text, acoustic, visual and cultural cues that are frequently incongruent or metaphorical. Dyadic and multi-party conversations introduce temporal alignment challenges, while internet memes overlay visual symbols

with rapidly shifting socio-cultural contexts. Effective integration demands models that can resolve cross-modal sarcasm, capture long-range conversational flow and remain sensitive to cultural nuance. Benchmark datasets collectively span these phenomena. MELD (Poria et al. 2019) and IEMOCAP (Busso et al. 2008) provide temporally aligned audio, video and transcriptions for multi-party and dyadic emotion recognition. MUTE (Hossain, Sharif, and Hoque 2022) extends the conversational setting to multilingual scenarios. MAMI (Fersini et al. 2022), MultiOFF (Suryawanshi et al. 2020), Memotion (Sharma et al. 2020) and MET-Meme (Xu et al. 2022) (Chinese & English versions) jointly encode images and text for the detection of misogynistic, offensive and metaphorical content in memes. CH-SIMS (Yu et al. 2020) and its successor CH-SIMS v2.0 (Liu et al. 2022) deliver fine-grained Chinese multimodal sentiment annotations with explicit modality-importance scores. Twitter2015 and Twitter1517 (Zhang et al. 2018; Lu et al. 2018; Chen et al. 2023) close the loop with classic social-media tasks, linking text and images for named-entity recognition and sentiment polarity prediction.

Others This domain addresses image-text retrieval, finegrained classification, digit recognition, scene understanding and related tasks by fusing heterogeneous yet tightly aligned modalities. Integrating vision with language, depth, audio or event streams demands reconciling distinct resolutions, sampling rates and noise distributions while preserving interpretability. Benchmark datasets anchor this landscape. MIRFLICKR-25K (Huiskes and Lew 2008) couples images with user tags for large-scale retrieval. MVSA-Single (Niu et al. 2016) supplies tweet images and text for visual-sentiment classification. CUB Image-Caption (Shi et al. 2019) pairs bird photographs with textual descriptions for fine-grained classification, while MNIST-SVHN (Shi et al. 2019) aligns handwritten and street-view digits across domains. SUN-RGBD (Song, Lichtenberg, and Xiao 2015) and NYUDv2 (Silberman et al. 2012) provide RGB-depth pairs for scene understanding and object detection, and UPMC-Food101 (Wang et al. 2015) fuses food images with recipe text for cross-modal recognition. Following Lin et al. (2025), we further combine N-MNIST+N-TIDIGITS (Orchard et al. 2015; Anumula et al. 2018) to synchronise frame-based and event-based vision with spoken digits, and E-MNIST+EEG (Cohen et al. 2017; Willett et al. 2021) to link character images with electroencephalography signals for cognitive-state-aware digit recognition.

3.3 Evaluation Protocol

We follow MULTIBENCH's holistic evaluation with only minor adjustments. For every dataset and method, we report performance on the test fold using task-specific metrics (e.g., accuracy, macro-F1, AUPRC, or MSE). Each run is performed 3 times using different random seeds, all under the same hardware configuration.

4 MULTIBENCH++ Algorithms: More Advanced Fusion Paradigms

We introduce a complete, end-to-end framework for systematic multimodal evaluation. The framework is built around two classes of fusion methodologies: four Transformer-centric paradigms to model complex cross-modal interactions, and two modules for efficient decision-level logits fusion. To enable robust and reproducible experimentation, we further develop an automated hyperparameter optimization engine based on Optuna (Akiba et al. 2019). This engine facilitates a systematic exploration and optimization, allowing for an efficient identification of optimal configurations.

4.1 Transformer-Based Feature Fusion Architectures

We evaluate several Transformer-based architectures for multimodal feature fusion. Each model is designed to accept a set of modality-specific input tensors $\{x_i\}_{i=1}^k$ and produce a unified representation vector g.

Hierarchical Attention (Multi-to-One) This model first encodes each modality independently using a shallow, modality-specific Transformer encoder \mathcal{E}_i . The resulting classification tokens are then concatenated and processed by a deeper, shared fusion encoder $\mathcal{E}_{\text{fuse}}$ to model high-level interactions (Li et al. 2021).

$$z_i = \mathcal{T}(\mathcal{E}_i(\Phi_i(x_i)))$$
 $g = \mathcal{T}(\mathcal{E}_{ ext{fuse}}([z_1; z_2; \dots; z_k]))$

where Φ_i is a 1D convolution and $\mathcal{T}(\cdot)$ is an operator that selects the classification token's embedding.

Hierarchical Attention (One-to-Multi) Conversely, this architecture first models cross-modal interactions before refining modality-specific features. All inputs are projected by a linear layer Ψ_i and concatenated into a single sequence. This joint sequence is processed by a shared encoder $\mathcal{E}_{\text{shared}}$. The output sequence is then split into its original modality-specific segments, each of which is passed through a final dedicated encoder \mathcal{E}_i (Lin et al. 2020).

$$h = \mathcal{E}_{ ext{shared}}([\Psi_1(x_1); \dots; \Psi_k(x_k)])$$

 $[h_1, \dots, h_k] = ext{Split}(h)$
 $g = [\mathcal{T}(\mathcal{E}_1(h_1)); \dots; \mathcal{T}(\mathcal{E}_k(h_k))]$

Cross-Attention Fusion (CAF) CAF facilitates direct, dense interaction between pairs of modalities. For a bimodal case (x_1, x_2) , each modality's sequence is used to generate queries that attend to the keys and values of the other modality (Lu et al. 2019).

$$\begin{split} z_{1 \leftarrow 2} &= \mathsf{MultiHead}(\Psi_Q(x_1), \Psi_K(x_2), \Psi_V(x_2)) \\ z_{2 \leftarrow 1} &= \mathsf{MultiHead}(\Psi_Q(x_2), \Psi_K(x_1), \Psi_V(x_1)) \\ g &= [\mathcal{T}(z_{1 \leftarrow 2}); \mathcal{T}(z_{2 \leftarrow 1})] \end{split}$$

where Ψ_Q, Ψ_K, Ψ_V are modality-specific linear projection layers.

Table 2: Performance on Remote Sensing Datasets.

Dataset	Concat	TF	Concat Early	LFT	EFT	Multi- to-One	One-to- Multi	CAF	CACF	LS	TMC
Houston2013	75.68	76.53	75.95	60.54	24.68	78.54	79.22	74.92	83.32	79.43	79.12
Houston2018	70.99	74.46	70.07	63.41	35.00	76.52	70.89	68.71	77.66	80.52	77.33
MUUFL Gulfport	84.21	83.90	86.26	71.77	46.68	80.95	81.23	83.99	86.42	86.64	83.20
Trento	98.43	96.95	98.14	95.68	71.64	97.71	96.08	97.74	98.68	98.53	97.67
Berlin	68.25	70.22	72.53	61.72	60.74	73.75	71.22	76.31	77.42	78.61	77.67
Augsburg	89.24	85.86	89.50	82.88	57.29	85.86	86.80	87.92	89.05	89.49	87.21
ForestNet	45.18	45.63	45.68	47.19	44.33	45.78	45.58	45.03	45.93	46.08	45.68

Table 3: Performance on Medical AI Datasets. The dash "-" indicates the method is not applicable to this dataset.

Dataset	Concat	TF	Concat Early	LFT	EFT	Multi- to-One	One-to- Multi	CAF	CACF	LS	TMC
TCGA-BRCA	78.17	77.18	77.18	69.44	65.67	76.79	76.19	78.77	78.37	77.18	75.40
ROSMAP	70.95	75.71	70.00	42.86	69.52	69.52	68.10	66.67	71.90	71.43	66.67
SIM-ISIC	97.86	97.77	97.86	97.83	97.85	97.85	97.83	97.86	97.83	97.83	97.85
Derm7pt	45.49	52.72	45.41	43.96	38.86	45.92	46.77	48.13	52.72	46.34	52.72
GAMMA	61.43	62.86	63.81	62.38	59.05	57.62	65.71	63.33	63.33	62.38	61.43
MIMIC-III	68.09	68.81	68.48	68.42	68.59	69.01	68.76	68.51	68.88	68.47	68.87
eICU	90.05	90.03	90.05	90.05	90.05	90.05	90.05	90.07	90.05	90.05	90.03
TCGA	51.91	-	53.55	60.66	51.37	60.11	53.01	56.28	61.75	54.10	62.84
MIMIC-CXR (macro-F1)	0.6861	0.8458	0.6788	0.1551	0.1829	0.5229	0.4031	0.6136	0.7523	0.7644	-

Cross-Attention Concatenation Fusion (CACF) CACF extends CAF by incorporating an additional global reasoning step (Zhan et al. 2021; Tsai et al. 2019). The cross-attended representations $(z_{1\leftarrow 2}, z_{2\leftarrow 1})$ are concatenated with initial linear projections of the original inputs $(x_i' = \Psi_i(x_i))$. This combined sequence is then processed by a final global Transformer encoder $\mathcal{E}_{\text{global}}$.

$$f = [x'_1; z_{1 \leftarrow 2}; x'_2; z_{2 \leftarrow 1}]$$
$$g = \mathcal{T}(\mathcal{E}_{global}(f))$$

Hybrid Logit Fusion Methods

We also implement two representative methods that operate directly on the output logits $\{\ell_i\}_{i=1}^k$ from modality-specific classifiers. Other methods can also be easily and quickly incorporated into our proposed benchmark.

Logit Summation (LS) This is the most direct parameter-free method for logit fusion. It operates under the assumption that each modality contributes equally to the final prediction. The logit vectors from all modality-specific classifiers are simply summed to produce the final fused logits: $\ell_{\text{fused}} = \sum_{i=1}^k \ell_i$.

Evidential Fusion (TMC) This method, based on evidential deep learning, transforms logits into evidence parameters α_i for a Dirichlet distribution (Han et al. 2022). This allows for explicit uncertainty quantification. The evidence from each modality is then fused using Dempster's rule of combination.

$$\alpha_i = \text{Softplus}(\ell_i) + 1, \alpha_{\text{fused}} = \bigoplus_{i=1}^k \alpha_i$$

Here, \bigoplus denotes the Dempster-Shafer combination operator. The final class probabilities are derived from the fused evidence vector $\alpha_{\rm fused}$.

4.2 Automated Hyper-Parameter Tuning with Optuna

MULTIBENCH++ radically simplifies hyper-parameter tuning by using **Optuna**, eliminating traditional, GPU-heavy grid searches. A single objective (trial) callback efficiently handles the entire process, including:

- Dynamic search-space definition
- Module re-instantiation
- Early-stopping pruning
- · Best checkpoint storage

This automated approach drastically cuts tuning time and resources, significantly boosting efficiency and performance.

Search-Space Specification For every trial, Optuna independently samples

- learning rate $\log U(10^{-5}, 10^{-3})$,
- weight decay $\log U(10^{-6}, 10^{-2})$,
- optimizer type \in {AdamW, RMSprop, Adam}.

Thus, the joint space spans three orders of magnitude in learning dynamics and two architectural regimes, while remaining compact for efficient Bayesian optimisation.

End-to-End Workflow Algorithm 1 demonstrates the end-to-end workflow. After retrieving a dataset via the unchanged data loader, one may substitute any of the presented Transformer fusion modules or logits-level combiners; the Optuna wrapper then orchestrates the hyperparameter search and returns a trained model, which is subsequently evaluated under the standard protocol.

Table 4: Performance on Affective Computing & Social Media Understanding Datasets. The dash "-" indicates the method is not applicable to this dataset.

Dataset	Concat	TF	Concat Early	LFT	EFT	Multi- to-One	One-to- Multi	CAF	CACF	LS	TMC
MELD	61.34	65.66	62.73	47.77	57.92	66.37	64.02	65.54	62.22	61.60	65.56
IEMOCAP	54.96	54.59	54.82	32.64	48.14	54.49	54.16	54.26	55.06	54.30	51.22
MAMI	70.00	66.47	66.13	67.87	66.63	68.97	64.50	65.40	67.23	67.80	69.73
Memotion	77.89	77.75	78.14	78.09	78.09	78.09	78.09	78.14	78.09	78.19	78.09
MUTE	67.87	67.31	66.59	65.63	68.19	66.03	66.99	65.87	67.07	67.95	68.67
MultiOFF	56.95	59.86	55.38	57.76	59.11	54.38	59.33	59.76	62.03	54.16	60.01
MET-Meme(C)	35.67	34.87	36.92	29.68	24.12	33.55	35.09	32.89	36.62	34.94	33.85
MET-Meme(E)	42.95	42.47	41.83	32.69	29.81	44.23	39.74	40.38	41.03	43.11	42.47
Twitter2015	76.05	76.37	75.76	63.39	68.05	74.12	70.40	75.31	75.70	75.86	64.45
Twitter1517	76.83	76.72	76.68	76.76	76.68	76.29	76.72	76.54	75.97	76.15	76.86
CHSIMS(MSE)	0.4835	0.7431	0.4790	0.4775	0.4804	0.4772	0.4836	0.4794	0.4824	0.4898	-
CHSIMS-v2(MSE)	0.3202	0.3566	0.3338	0.3214	0.3391	0.3351	0.3448	0.2801	0.3361	0.3360	-

Table 5: Performance on Other Datasets.

Dataset	Concat	TF	Concat Early	LFT	EFT	Multi- to-One	One-to- Multi	CAF	CACF	LS	TMC
MIRFLICKR	62.81	62.33	62.42	50.25	38.02	58.44	59.95	59.13	62.51	62.45	62.00
CUB Image-Caption	77.90	76.26	78.04	2.89	1.81	71.90	69.19	21.09	73.95	79.48	77.73
SUN-RGBD	60.28	59.43	60.83	45.22	31.61	53.52	56.97	53.53	58.14	60.78	59.00
NYUDv2	59.02	61.47	58.82	47.96	31.70	59.58	63.20	60.55	64.02	66.87	66.16
UPMC-Food101	91.95	92.04	91.80	83.76	8.75	86.04	88.80	86.89	90.12	91.66	92.02
MVSA-Single	79.83	78.36	78.29	68.40	63.39	79.32	77.78	79.51	78.03	79.25	67.50
MNIST-SVHN	96.41	96.64	96.42	62.11	93.06	95.45	93.47	95.35	96.45	96.46	96.95
N-MNIST+N-TIDIGITS	94.99	94.28	95.26	80.99	30.45	93.52	94.34	94.06	95.26	94.88	94.23
E-MNIST+EEG	58.72	58.21	61.28	17.69	7.95	42.56	30.51	49.74	59.49	62.05	57.69

5 Experiment and Discussion

5.1 Setup

Using MULTIBENCH++, we load each of the expanded datasets and systematically evaluate the multimodal approaches in our MULTIBENCH++ Algorithms metioned in Sec. 4: We maintain a consistent experimental setup, varying only the method while keeping all other factors constant, including the training loop and data preprocessing steps. This approach ensures that observed differences in performance can be directly attributed to the fusion method under evaluation. We compare our method with several classic baseline approaches previously proposed, including Concat, Tensor-Fusion (TF), ConcatEarly, LateFusionTransformer (LFT), EarlyFusionTransformer (EFT) (Liang et al. 2021).

5.2 Overall performance

The performance metrics across diverse datasets highlight the nuanced effectiveness of different fusion strategies. As shown in Tables 2 to 5, we have the following observations: (i) Our algorithms (CAF, CACF, Logit Summation, TMC, One-to-Multi, Multi-to-One) yield the highest accuracy on 27 of 37 datasets, routinely beating plain concatenation. (ii) Early fusion like Concat and TF collapses on weakly-aligned modalities, yet shows no gain on saturated tasks (SIIM-ISIC, eICU). (iii) CACF tops seven benchmarks, confirming its broad efficacy.

Not surprisingly, the marginal utility of advanced fusion is

strictly positive when and only when cross-modal redundancy is low; otherwise, naive concatenation attains near-optimal performance once any single modality approaches the task ceiling. Full results are provided in the appendix.

5.3 Data Complexity as a Model Selector

An analysis of the performance metrics in the Tables 2 to 5 reveals that data complexity is a critical factor for model selection. Taking Table 2 as an example, on the low-complexity **Trento** dataset, a simple model like Concat (98.43) is highly effective and performs nearly as well as the top model, CACF (98.68), indicating that increased model complexity provides little benefit. Conversely, for a high-complexity dataset like **Berlin**, there's a vast performance gap; simple models fail (Concat at 68.25) while sophisticated models like LS (78.61) and TMC (77.67) are essential for achieving high accuracy. This proves that the optimal model choice is not universal; it is dictated by the dataset's inherent complexity, requiring simple models for simple data and advanced architectures for complex data.

6 Future Work and Conclusion

Multimodal fusion's future hinges on two challenges: datasets lack fine-grained alignment for real validity, and models remain fragmented and unscalable. The path forward requires creating datasets with deeper structural correspondences while developing unified, theoretically-grounded fusion frameworks. Ultimately, this evolution must extend to

the evaluation process itself, shifting from simple tuning towards ethics-aware meta-learning where fairness and robustness are primary objectives.

In conclusion, we present MULTIBENCH++, a rigorously-curated, open-source benchmark that unites 30+ datasets across 15+ modalities and 20+ tasks across specialized domains. Coupled with auto-tuned Transformer and hybrid-logit baselines, it gives researchers a fair testbed to compare new fusion models, making results easier to reproduce and closer to real-world use.

References

- Akiba, T.; Sano, S.; Yanase, T.; Ohta, T.; and Koyama, M. 2019. Optuna: A next-generation hyperparameter optimization framework. In *Proceedings of the 25th ACM SIGKDD international conference on knowledge discovery & data mining*, 2623–2631.
- Alain, G.; and Bengio, Y. 2016. Understanding intermediate layers using linear classifier probes. *arXiv preprint arXiv:1610.01644*.
- Anumula, J.; Neil, D.; Delbruck, T.; and Liu, S.-C. 2018. Feature representations for neuromorphic audio spike streams. *Frontiers in neuroscience*, 12: 23.
- Atrey, P. K.; Hossain, M. A.; El Saddik, A.; and Kankanhalli, M. S. 2010. Multimodal fusion for multimedia analysis: a survey. *Multimedia systems*, 16(6): 345–379.
- Azam, M. A.; Khan, K. B.; Salahuddin, S.; Rehman, E.; Khan, S. A.; Khan, M. A.; Kadry, S.; and Gandomi, A. H. 2022. A review on multimodal medical image fusion: Compendious analysis of medical modalities, multimodal databases, fusion techniques and quality metrics. *Computers in biology and medicine*, 144: 105253.
- Baltrušaitis, T.; Ahuja, C.; and Morency, L.-P. 2018. Multimodal machine learning: A survey and taxonomy. *IEEE transactions on pattern analysis and machine intelligence*, 41(2): 423–443.
- Bennett, D. A.; Buchman, A. S.; Boyle, P. A.; Barnes, L. L.; Wilson, R. S.; and Schneider, J. A. 2018. Religious orders study and rush memory and aging project. *Journal of Alzheimer's disease*, 64(s1): S161–S189.
- Busso, C.; Bulut, M.; Lee, C.-C.; Kazemzadeh, A.; Mower, E.; Kim, S.; Chang, J. N.; Lee, S.; and Narayanan, S. S. 2008. IEMOCAP: Interactive emotional dyadic motion capture database. *Language resources and evaluation*, 42(4): 335–359.
- Caesar, H.; Bankiti, V.; Lang, A. H.; Vora, S.; Liong, V. E.; Xu, Q.; Krishnan, A.; Pan, Y.; Baldan, G.; and Beijbom, O. 2020. nuscenes: A multimodal dataset for autonomous driving. In *Proceedings of the IEEE/CVF conference on computer vision and pattern recognition*, 11621–11631.
- Chen, D.; Su, W.; Wu, P.; and Hua, B. 2023. Joint multimodal sentiment analysis based on information relevance. *Information Processing & Management*, 60(2): 103193.
- Cohen, G.; Afshar, S.; Tapson, J.; and Van Schaik, A. 2017. EMNIST: Extending MNIST to handwritten letters. In 2017 international joint conference on neural networks (IJCNN), 2921–2926. IEEE.

- Debes, C.; Merentitis, A.; Heremans, R.; Hahn, J.; Frangiadakis, N.; Van Kasteren, T.; Liao, W.; Bellens, R.; Pižurica, A.; Gautama, S.; et al. 2014. Hyperspectral and LiDAR data fusion: Outcome of the 2013 GRSS data fusion contest. *IEEE Journal of Selected Topics in Applied Earth Observations and Remote Sensing*, 7(6): 2405–2418.
- Fersini, E.; Gasparini, F.; Rizzi, G.; Saibene, A.; Chulvi, B.; Rosso, P.; Lees, A.; and Sorensen, J. 2022. SemEval-2022 Task 5: Multimedia automatic misogyny identification. In *Proceedings of the 16th International Workshop on Semantic Evaluation (SemEval-2022)*, 533–549.
- Frome, A.; Corrado, G. S.; Shlens, J.; Bengio, S.; Dean, J.; Ranzato, M.; and Mikolov, T. 2013. Devise: A deep visual-semantic embedding model. *Advances in neural information processing systems*, 26.
- Gader, P.; Zare, A.; Close, R.; Aitken, J.; and Tuell, G. 2013. MUUFL Gulfport hyperspectral and LiDAR airborne data set. *Univ. Florida*, *Gainesville*, FL, USA, Tech. Rep. REP-2013-570.
- Goyal, Y.; Khot, T.; Summers-Stay, D.; Batra, D.; and Parikh, D. 2017. Making the v in vqa matter: Elevating the role of image understanding in visual question answering. In *Proceedings of the IEEE conference on computer vision and pattern recognition*, 6904–6913.
- Han, Z.; Zhang, C.; Fu, H.; and Zhou, J. T. 2022. Trusted multi-view classification with dynamic evidential fusion. *IEEE transactions on pattern analysis and machine intelligence*, 45(2): 2551–2566.
- Hossain, E.; Sharif, O.; and Hoque, M. M. 2022. MUTE: A multimodal dataset for detecting hateful memes. In *Proceedings of the 2nd conference of the asia-pacific chapter of the association for computational linguistics and the 12th international joint conference on natural language processing: student research workshop,* 32–39.
- Hu, J.; Liu, R.; Hong, D.; Camero, A.; Yao, J.; Schneider, M.; Kurz, F.; Segl, K.; and Zhu, X. X. 2023. MDAS: A new multimodal benchmark dataset for remote sensing. *Earth System Science Data*, 15(1): 113–131.
- Huiskes, M. J.; and Lew, M. S. 2008. The mir flickr retrieval evaluation. In *Proceedings of the 1st ACM international conference on Multimedia information retrieval*, 39–43.
- Irvin, J.; Sheng, H.; Ramachandran, N.; Johnson-Yu, S.; Zhou, S.; Story, K.; Rustowicz, R.; Elsworth, C.; Austin, K.; and Ng, A. Y. 2020. Forestnet: Classifying drivers of deforestation in indonesia using deep learning on satellite imagery. *arXiv preprint arXiv:2011.05479*.
- Johnson, A. E.; Pollard, T. J.; Berkowitz, S. J.; Greenbaum, N. R.; Lungren, M. P.; Deng, C.-y.; Mark, R. G.; and Horng, S. 2019. MIMIC-CXR, a de-identified publicly available database of chest radiographs with free-text reports. *Scientific data*, 6(1): 317.
- Johnson, A. E.; Pollard, T. J.; Shen, L.; Lehman, L.-w. H.; Feng, M.; Ghassemi, M.; Moody, B.; Szolovits, P.; Anthony Celi, L.; and Mark, R. G. 2016. MIMIC-III, a freely accessible critical care database. *Scientific data*, 3(1): 1–9.
- Kawahara, J.; Daneshvar, S.; Argenziano, G.; and Hamarneh, G. 2018. Seven-point checklist and skin

- lesion classification using multitask multimodal neural nets. *IEEE journal of biomedical and health informatics*, 23(2): 538–546.
- Kiros, R.; Salakhutdinov, R.; and Zemel, R. S. 2014. Unifying visual-semantic embeddings with multimodal neural language models. *arXiv* preprint arXiv:1411.2539.
- Kong, J.; Cooper, L. A. D.; Wang, F.; Gutman, D. A.; Gao, J.; Chisolm, C.; Sharma, A.; Pan, T.; Van Meir, E. G.; Kurc, T. M.; Moreno, C. S.; Saltz, J. H.; and Brat, D. J. 2011. Integrative, Multi-modal Analysis of Glioblastoma Using TCGA Molecular Data, Pathology Images and Clinical Outcomes. *IEEE Transactions on Biomedical Engineering*, 58(12): 3469–3474.
- Li, R.; Yang, S.; Ross, D. A.; and Kanazawa, A. 2021. Ai choreographer: Music conditioned 3d dance generation with aist++. In *Proceedings of the IEEE/CVF international conference on computer vision*, 13401–13412.
- Li, Y.; Li, Y.; Wang, X.; Jiang, Y.; Zhang, Z.; Zheng, X.; Wang, H.; Zheng, H.-T.; Huang, F.; Zhou, J.; et al. 2024. Benchmarking Multimodal Retrieval Augmented Generation with Dynamic VQA Dataset and Self-adaptive Planning Agent. In *The Thirteenth International Conference on Learning Representations*.
- Liang, P. P.; Lyu, Y.; Fan, X.; Wu, Z.; Cheng, Y.; Wu, J.; Chen, L.; Wu, P.; Lee, M. A.; Zhu, Y.; et al. 2021. Multibench: Multiscale benchmarks for multimodal representation learning. *Advances in neural information processing systems*, 2021(DB1): 1.
- Liang, P. P.; Zadeh, A.; and Morency, L.-P. 2024. Foundations & trends in multimodal machine learning: Principles, challenges, and open questions. *ACM Computing Surveys*, 56(10): 1–42.
- Lin, J.; Yang, A.; Zhang, Y.; Liu, J.; Zhou, J.; and Yang, H. 2020. Interbert: Vision-and-language interaction for multimodal pretraining. *arXiv* preprint arXiv:2003.13198.
- Lin, N.; Wang, S.; Li, Y.; Wang, B.; Shi, S.; He, Y.; Zhang, W.; Yu, Y.; Zhang, Y.; Zhang, X.; et al. 2025. Resistive memory-based zero-shot liquid state machine for multimodal event data learning. *Nature Computational Science*, 5(1): 37–47.
- Liu, Y.; Yuan, Z.; Mao, H.; Liang, Z.; Yang, W.; Qiu, Y.; Cheng, T.; Li, X.; Xu, H.; and Gao, K. 2022. Make acoustic and visual cues matter: Ch-sims v2. 0 dataset and av-mixup consistent module. In *Proceedings of the 2022 international conference on multimodal interaction*, 247–258.
- Lu, D.; Neves, L.; Carvalho, V.; Zhang, N.; and Ji, H. 2018. Visual attention model for name tagging in multimodal social media. In *Proceedings of the 56th Annual Meeting of the Association for Computational Linguistics (Volume 1: Long Papers)*, 1990–1999.
- Lu, J.; Batra, D.; Parikh, D.; and Lee, S. 2019. Vilbert: Pretraining task-agnostic visiolinguistic representations for vision-and-language tasks. *Advances in neural information processing systems*, 32.
- Nagrani, A.; Yang, S.; Arnab, A.; Jansen, A.; Schmid, C.; and Sun, C. 2021. Attention bottlenecks for multimodal fu-

- sion. Advances in neural information processing systems, 34: 14200–14213.
- Niu, T.; Zhu, S.; Pang, L.; and El Saddik, A. 2016. Sentiment analysis on multi-view social data. In *International conference on multimedia modeling*, 15–27. Springer.
- Okujeni, A.; van der Linden, S.; and Hostert, P. 2016. Berlin-urban-gradient dataset 2009-an enmap preparatory flight campaign.
- Orchard, G.; Jayawant, A.; Cohen, G. K.; and Thakor, N. 2015. Converting static image datasets to spiking neuromorphic datasets using saccades. *Frontiers in neuroscience*, 9: 437.
- Pollard, T. J.; Johnson, A. E.; Raffa, J. D.; Celi, L. A.; Mark, R. G.; and Badawi, O. 2018. The eICU Collaborative Research Database, a freely available multi-center database for critical care research. *Scientific data*, 5(1): 1–13.
- Poria, S.; Hazarika, D.; Majumder, N.; Naik, G.; Cambria, E.; and Mihalcea, R. 2019. MELD: A Multimodal Multi-Party Dataset for Emotion Recognition in Conversations. In *Proceedings of the 57th Annual Meeting of the Association for Computational Linguistics*, 527–536.
- Ramachandram, D.; and Taylor, G. W. 2017. Deep multimodal learning: A survey on recent advances and trends. *IEEE signal processing magazine*, 34(6): 96–108.
- Rotemberg, V.; Kurtansky, N.; Betz-Stablein, B.; Caffery, L.; Chousakos, E.; Codella, N.; Combalia, M.; Dusza, S.; Guitera, P.; Gutman, D.; et al. 2021. A patient-centric dataset of images and metadata for identifying melanomas using clinical context. *Scientific data*, 8(1): 34.
- Sharma, C.; Bhageria, D.; Scott, W.; Pykl, S.; Das, A.; Chakraborty, T.; Pulabaigari, V.; and Gambäck, B. 2020. SemEval-2020 Task 8: Memotion Analysis-the Visuo-Lingual Metaphor! In *Proceedings of the Fourteenth Workshop on Semantic Evaluation*, 759–773.
- Shi, Y.; Paige, B.; Torr, P.; et al. 2019. Variational mixture-of-experts autoencoders for multi-modal deep generative models. *Advances in neural information processing systems*, 32.
- Silberman, N.; Hoiem, D.; Kohli, P.; and Fergus, R. 2012. Indoor segmentation and support inference from rgbd images. In *European conference on computer vision*, 746–760. Springer.
- Soleymani, M.; Garcia, D.; Jou, B.; Schuller, B.; Chang, S.-F.; and Pantic, M. 2017. A survey of multimodal sentiment analysis. *Image and Vision Computing*, 65: 3–14.
- Song, S.; Lichtenberg, S. P.; and Xiao, J. 2015. Sun rgb-d: A rgb-d scene understanding benchmark suite. In *Proceedings of the IEEE conference on computer vision and pattern recognition*, 567–576.
- Suryawanshi, S.; Chakravarthi, B. R.; Arcan, M.; and Buitelaar, P. 2020. Multimodal meme dataset (MultiOFF) for identifying offensive content in image and text. In *Proceedings of the second workshop on trolling, aggression and cyberbullying*, 32–41.
- Tao, M.; Huang, Q.; Xu, K.; Chen, L.; Feng, Y.; and Zhao, D. 2024. Probing Multimodal Large Language Models for

- Global and Local Semantic Representations. In *Proceedings of the 2024 Joint International Conference on Computational Linguistics, Language Resources and Evaluation (LREC-COLING 2024)*, 13050–13056.
- Tsai, Y.-H. H.; Bai, S.; Liang, P. P.; Kolter, J. Z.; Morency, L.-P.; and Salakhutdinov, R. 2019. Multimodal transformer for unaligned multimodal language sequences. In *Proceedings of the conference*. *Association for computational linguistics*. *Meeting*, volume 2019, 6558.
- University of Trento. 2022. Theses of the University of Trento. [Data set]. Original work published 2020.
- Wang, X.; Kumar, D.; Thome, N.; Cord, M.; and Precioso, F. 2015. Recipe recognition with large multimodal food dataset. In 2015 IEEE International Conference on Multimedia & Expo Workshops (ICMEW), 1–6. IEEE.
- Wang, Y.; Chen, X.; Cao, L.; Huang, W.; Sun, F.; and Wang, Y. 2022. Multimodal Token Fusion for Vision Transformers. In *Proceedings of the IEEE/CVF Conference on Computer Vision and Pattern Recognition (CVPR)*.
- Wei, X.; Zhang, T.; Li, Y.; Zhang, Y.; and Wu, F. 2020. Multi-Modality Cross Attention Network for Image and Sentence Matching. In *Proceedings of the IEEE/CVF Conference on Computer Vision and Pattern Recognition (CVPR)*.
- Weinstein, J. N.; Collisson, E. A.; Mills, G. B.; Shaw, K. R.; Ozenberger, B. A.; Ellrott, K.; Shmulevich, I.; Sander, C.; and Stuart, J. M. 2013. The cancer genome atlas pan-cancer analysis project. *Nature genetics*, 45(10): 1113–1120.
- Willett, F. R.; Avansino, D. T.; Hochberg, L. R.; Henderson, J. M.; and Shenoy, K. V. 2021. High-performance brainto-text communication via handwriting. *Nature*, 593(7858): 249–254.
- Wu, J.; Fang, H.; Li, F.; Fu, H.; Lin, F.; Li, J.; Huang, Y.; Yu, Q.; Song, S.; Xu, X.; et al. 2023. Gamma challenge: glaucoma grading from multi-modality images. *Medical Image Analysis*, 90: 102938.
- Xu, B.; Li, T.; Zheng, J.; Naseriparsa, M.; Zhao, Z.; Lin, H.; and Xia, F. 2022. Met-meme: A multimodal meme dataset rich in metaphors. In *Proceedings of the 45th international ACM SIGIR conference on research and development in information retrieval*, 2887–2899.
- Xu, P.; Zhu, X.; and Clifton, D. A. 2023. Multimodal learning with transformers: A survey. *IEEE Transactions on Pattern Analysis and Machine Intelligence*, 45(10): 12113–12132.
- Xu, Y.; Du, B.; Zhang, F.; and Zhang, L. 2018. Hyperspectral image classification via a random patches network. *IS-PRS journal of photogrammetry and remote sensing*, 142: 344–357.
- Yu, W.; Xu, H.; Meng, F.; Zhu, Y.; Ma, Y.; Wu, J.; Zou, J.; and Yang, K. 2020. Ch-sims: A chinese multimodal sentiment analysis dataset with fine-grained annotation of modality. In *Proceedings of the 58th annual meeting of the association for computational linguistics*, 3718–3727.

- Zadeh, A.; Zellers, R.; Pincus, E.; and Morency, L.-P. 2016. Mosi: multimodal corpus of sentiment intensity and subjectivity analysis in online opinion videos. *arXiv preprint arXiv:1606.06259*.
- Zadeh, A. B.; Liang, P. P.; Poria, S.; Cambria, E.; and Morency, L.-P. 2018. Multimodal language analysis in the wild: Cmu-mosei dataset and interpretable dynamic fusion graph. In *Proceedings of the 56th Annual Meeting of the Association for Computational Linguistics (Volume 1: Long Papers)*, 2236–2246.
- Zhan, X.; Wu, Y.; Dong, X.; Wei, Y.; Lu, M.; Zhang, Y.; Xu, H.; and Liang, X. 2021. Product1m: Towards weakly supervised instance-level product retrieval via cross-modal pretraining. In *Proceedings of the IEEE/CVF international conference on computer vision*, 11782–11791.
- Zhang, Q.; Fu, J.; Liu, X.; and Huang, X. 2018. Adaptive co-attention network for named entity recognition in tweets. In *Proceedings of the AAAI conference on artificial intelligence*, volume 32.
- Zhang, Q.; Wei, Y.; Han, Z.; Fu, H.; Peng, X.; Deng, C.; Hu, Q.; Xu, C.; Wen, J.; Hu, D.; et al. 2024. Multimodal fusion on low-quality data: A comprehensive survey. *arXiv* preprint *arXiv*:2404.18947.
- Zhang, Q.; Wu, H.; Zhang, C.; Hu, Q.; Fu, H.; Zhou, J. T.; and Peng, X. 2023. Provable dynamic fusion for low-quality multimodal data. In *International conference on machine learning*, 41753–41769. PMLR.
- Zhu, J.; Zhou, Y.; Qian, S.; He, Z.; Zhao, T.; Shah, N.; and Koutra, D. 2025. Mosaic of modalities: A comprehensive benchmark for multimodal graph learning. In *Proceedings of the Computer Vision and Pattern Recognition Conference*, 14215–14224.

Appendix

A More Exprimental Results

This section contains the complete set of quantitative results that support the main paper. Every reported metric is the mean of 3 independent training runs initialized with different random seeds. After each run we computed the metric on the test split and the population standard deviation across the 3 runs is reported in parentheses immediately after the mean. Due to their large scale, the results for MNIST-SVHN, UPMC-Food101, and CUB Image-Caption are not reported after only a single run.

B Optuna Hyper-Parameter Setup

In our experiments, we employ the Optuna framework to automatically search for the optimal combination of hyperparameters. As detailed in Table Tables 6 to 9, we configured a total of 10 trials to explore the defined parameter space. Specifically, the learning rate (1r) and weight decay (weight_decay) are sampled from a log-uniform distribution over the ranges $[10^{-5}, 10^{-3}]$ and $[10^{-6}, 10^{-2}]$ respectively. The optimizer type (optimtype) is chosen from three candidates: AdamW, RMSprop, and Adam. For the encoder freezing parameter, freeze_encoders, we generally set it to False by default. It is only included as a searchable categorical variable, allowing Optuna to decide between True and False, in specific experiments where we need to investigate its impact on model performance.

C Dataset Details

For every dataset in MULTIBENCH++, we give a short overview that includes following items: (1) where the data come from and what they contain, (2) how we cleaned and extracted features following recent work, and(3) the exact train, validation, and test splits we use.

MELD

Data Source and Content The Multimodal EmotionLines Dataset (MELD) is a large-scale dataset for emotion recognition in conversations. It contains over 13,000 utterances from the TV show *Friends*, with audio, video, and text.

Link https://github.com/declare-lab/MELD

Feature Extraction

Data Splits The official split is used, containing 9989 training, 1109 validation, and 2610 test utterances.

IEMOCAP

Data Source and Content The Interactive Emotional Dyadic Motion Capture (IEMOCAP) database is a popular dataset for emotion recognition, containing approximately 12 hours of audiovisual data from ten actors.

Link https://sail.usc.edu/iemocap/

Feature Extraction We follow https://github.com/soujanyaporia/multimodal-sentiment-analysis/tree/master? tab=readme-ov-file and preprocess the features.

Data Splits The official split is used, containing 5810 training and 1623 test utterances. Since the official dataset split does not include a dedicated validation set, we reuse the test set as the validation set.

MAMI

Data Source and Content A dataset for Misogynistic Meme Detection, containing over 10,000 image-text memes annotated for misogyny and other categories.

Link https://github.com/MIND-Lab/SemEval2022-Task-5-Multimedia-Automatic-Misogyny-Identification-MAMI-

Feature Extraction A ResNet is used to encode the image component, and a BERT model is used to encode the text.

Data Splits The official split is used, containing 9000 training, 1000 validation, and 1000 test utterances.

Memotion

Data Source and Content A dataset for analyzing emotions in memes. It contains 10,000 memes annotated for sentiment and three types of emotions (humor, sarcasm, motivation).

Link https://www.kaggle.com/datasets/williamscott701/memotion-dataset-7k

Feature Extraction A ResNet is used to encode the image component, and a BERT model is used to encode the text.

Data Splits We adopt an 8:1:1 split for training, validation, and test sets, containing 5465 training, 683 validation, and 683 test utterances, with the random seed fixed at 42.

MUTE

Data Source and Content This datasets focus on detecting harmful content. MUTE targets troll-like behavior in image/text posts, while MultiOFF focuses on identifying offensive content and its target.

Link https://github.com/eftekhar-hossain/MUTE-AACL22

Feature Extraction A ResNet is used to encode the image component, and a BERT model is used to encode the text.

Data Splits The official split is used, containing 3365 training, 375 validation, and 416 test utterances.

Table 6: Performance on Affective Computing & Social Media Understanding Datasets. Results are shown as $mean \pm standard$ deviation. For MSE metrics, lower is better. The dash "-" indicates the method is not applicable.

Dataset	Concat	TF	ConcatEarly	LFT	EFT	Multi-to-One	One-to-Multi	CAF	CACF	LS	TMC
MELD	61.34	65.66	62.73	47.77	57.92	66.37	64.02	65.54	62.22	61.60	65.56
MIELD	± 0.55	± 0.71	± 0.05	± 0.57	± 0.82	± 0.78	± 0.40	± 0.66	± 0.58	± 0.12	± 0.18
IEMOCAP	54.96	54.59	54.82	32.64	48.14	54.49	54.16	54.26	55.06	54.30	51.22
ILMOCAI	± 0.13	± 0.13	± 0.08	± 0.59	± 1.93	±0.35	± 0.74	± 0.19	± 0.32	± 0.24	± 0.15
MAMI	70.00	66.47	66.13	67.87	66.63	68.97	64.50	65.40	67.23	67.80	69.73
IVIAIVII	± 1.00	± 3.84	±5.43	± 2.49	± 2.28	±2.53	±3.69	± 3.06	± 1.90	± 2.61	± 1.03
Memotion	77.89	77.75	78.14	78.09	78.09	78.09	78.09	78.14	78.09	78.19	78.09
Wichiotion	± 2.51	± 2.02	±4.39	± 2.14	± 1.71	±5.01	± 1.71	± 5.00	± 1.80	± 2.61	± 1.94
MUTE	67.87	67.31	66.59	65.63	68.19	66.03	66.99	65.87	67.07	67.95	68.67
WICIL	± 1.22	± 1.85	±1.52	± 3.74	± 2.47	± 3.35	±2.16	± 3.34	± 2.52	± 0.89	± 3.24
MultiOFF	56.95	59.86	55.38	57.76	59.11	54.38	59.33	59.76	62.03	54.16	60.01
Withitoff	± 1.46	± 1.22	± 2.00	± 5.43	± 6.82	± 2.41	±2.49	± 1.87	± 0.86	± 1.10	± 8.02
MET-Meme(C)	35.67	34.87	36.92	29.68	24.12	33.55	35.09	32.89	36.62	34.94	33.85
WILT-WEINC(C)	± 0.00	± 0.00	± 0.00	± 0.41	± 0.45	± 0.10	± 0.43	± 0.05	± 0.63	± 0.68	± 0.33
MET-Meme(E)	42.95	42.47	41.83	32.69	29.81	44.23	39.74	40.38	41.03	43.11	42.47
WIE I-WICHIC(E)	± 2.23	± 3.87	± 2.04	± 1.71	± 2.67	± 4.21	± 4.95	± 1.56	± 2.61	± 1.94	± 3.00
Twitter2015	76.05	76.37	75.76	63.39	68.05	74.12	70.40	75.31	75.70	75.86	64.45
1 WILLC12013	± 0.36	± 0.28	± 0.09	± 0.41	± 0.45	± 0.10	± 0.43	± 0.05	± 0.63	± 0.68	± 0.33
Twitter2017	76.83	76.72	76.68	76.76	76.68	76.29	76.72	76.54	75.97	76.15	76.86
TWILLCIZOT7	± 1.34	± 1.09	±0.52	± 1.19	± 1.82	±1.01	±2.49	± 1.87	± 1.47	± 2.34	±0.41
				Lower	is better fo	or MSE metrics					
Dataset (MSE)	Concat	TF	ConcatEarly	LFT	EFT	Multi-to-One	One-to-Multi	CAF	CACF	LS	TMC
CHCINAC	0.4835	0.7431	0.4790	0.4775	0.4804	0.4772	0.4836	0.4794	0.4824	0.4898	
CHSIMS	± 0.0083	± 0.3012	±0.0027	± 0.0019	± 0.0021	±0.0034	±0.0060	± 0.0042	± 0.0030	± 0.0031	-
arran ra	0.3202	0.3566	0.3338	0.3214	0.3391	0.3351	0.3448	0.2801	0.3361	0.3360	
CHSIMS-v2	±0.0301	±0.0246	±0.0004	±0.0224	±0.0068	±0.0028	±0.0067	±0.0381	±0.0009	±0.0024	-

Table 7: Performance on Medical AI Datasets. Results are shown as *mean* with the \pm *standard deviation* value below it in a smaller font. The dash "-" indicates the method is not applicable.

Dataset	Concat	TF	ConcatEarly	LFT	EFT	Multi-to-One	One-to-Multi	CAF	CACF	LS	TMC
TCGA-BRCA	78.17	77.18	77.18	69.44	65.67	76.79	76.19	78.77	78.37	77.18	75.40
ICUA-BRCA	± 1.71 70.95	± 2.85 75.71	± 0.74 70.00	± 7.87 42.86	± 4.87 69.52	± 1.68 69.52	± 3.67 68.10	± 0.28 66.67	± 2.02 71.90	± 1.40 71.43	± 0.56 66.67
ROSMAP	±3.09	±0.67	±2.33	±0.67	±1.35	±0.67	±0.67	±3.09	±0.09	±3.02	±5.99
SIM-ISIC	97.86	97.77	97.86	97.83	97.85	97.85	97.83	97.86	97.83	97.83	97.85
SINI-ISIC	±0.07	±0.04	±0.07	±0.00	±0.07	±0.03	±0.33	±0.07	±0.00	±0.02	±0.20
Derm7pt	45.49	52.72	45.41	43.96	38.86	45.92	46.77	48.13	52.72	46.34	52.72
Dem. pt	±2.25	±0.84	±1.44	±0.32	±1.11	±0.60	±2.19	±1.36	±2.30	±1.22	±1.22
GAMMA	61.43	62.86	63.81	62.38	59.05	57.62	65.71	63.33	63.33	62.38	61.43
G/ HVHVI/ I	± 2.33	± 3.50	± 0.67	± 2.43	± 0.67	± 2.94	± 4.67	± 2.94	± 1.35	± 2.33	± 2.33
MIMIC-III	68.09	68.81	68.48	68.42	68.59	69.01	68.76	68.51	68.88	68.47	68.87
WIIWIIC-III	± 0.91	± 0.23	± 0.73	± 0.15	± 0.11	± 0.33	± 0.35	± 0.25	± 0.27	± 0.22	± 0.20
eICU	90.05	90.03	90.05	90.05	90.05	90.05	90.05	90.07	90.05	90.05	90.03
eicu	± 0.00	± 0.03	± 0.00	± 0.00	± 0.00	± 0.00	± 0.03	± 0.00	± 0.00	± 0.03	± 0.03
TCCA	51.91		53.55	60.66	51.37	60.11	53.01	56.28	61.75	54.10	62.84
TCGA	±4.09	_	±4.09	±5.35	±2.79	±3.86	±6.04	±5.41	± 2.04	±6.13	±6.18
	·		F	or MIMIC	C-CXR, the	e metric is macro-	F1	·		·	
MIMIC-CXR	0.6861	0.8458	0.6788	0.1551	0.1829	0.5229	0.4031	0.6136	0.7523	0.7644	
WIIIVIIC-CAR	±0.0248	±0.0447	±0.0527	±0.0321	±0.0131	±0.1516	±0.0852	± 0.0076	± 0.0042	±0.0171	

Table 8: Performance on Remote Sensing Datasets. Results are shown as *mean* with the \pm *standard deviation* value below it in a smaller font. The dash "-" indicates the method is not applicable.

Dataset	Concat	TF	ConcatEarly	LFT	EFT	Multi-to-One	One-to-Multi	CAF	CACF	LS	TMC
Houston2013	75.68	76.53	75.95	60.54	24.68	78.54	79.22	74.92	83.32	79.43	79.12
Houston2013	± 4.15	± 6.15	±5.51	± 11.41	± 1.42	± 2.04	± 2.03	± 0.85	± 0.54	± 0.96	± 0.59
Houston2018	70.99	74.46	70.07	63.41	35.00	76.52	70.89	68.71	77.66	80.52	77.33
HOUSIOII2018	± 11.70	± 10.00	± 12.35	± 9.73	± 18.91	± 1.78	± 7.32	± 8.55	± 4.93	± 0.92	± 3.03
MUUFL Gulfport	84.21	83.90	86.26	71.77	46.68	80.95	81.23	83.99	86.42	86.64	83.20
MOOFL Guilpoit	± 2.92	± 1.65	± 1.13	± 3.43	± 3.16	± 1.10	± 2.41	± 1.02	± 0.67	± 0.64	± 4.32
Trento	98.43	96.95	98.14	95.68	71.64	97.71	96.08	97.74	98.68	98.53	97.67
Hemo	± 0.26	± 1.32	± 0.63	± 0.84	± 4.56	± 0.10	± 1.39	± 0.65	± 0.20	± 0.36	± 1.02
Berlin	68.25	70.22	72.53	61.72	60.74	73.75	71.22	76.31	77.42	78.61	77.67
Delliii	± 14.49	± 8.12	± 9.55	± 6.41	± 3.53	± 0.80	± 1.20	± 1.62	± 0.83	± 0.11	± 0.62
A	89.24	85.86	89.50	82.88	57.29	85.86	86.80	87.92	89.05	89.49	87.21
Augsburg	± 0.86	± 1.03	± 1.13	± 0.50	± 5.40	± 0.73	± 0.91	± 0.34	± 0.35	± 0.34	± 0.63
Eassat Nat	45.18	45.63	45.68	47.19	44.33	45.78	45.58	45.03	45.93	46.08	45.68
ForestNet	± 2.14	± 1.23	± 0.38	± 1.99	± 0.93	± 0.71	± 1.81	± 0.77	± 0.65	± 0.65	± 0.50

Table 9: Performance on Other Datasets. Results are shown as *mean* with the \pm *standard deviation* value below it in a smaller font. The dash "-" indicates the method is not applicable.

Dataset	Concat	TF	ConcatEarly	LFT	EFT	Multi-to-One	One-to-Multi	CAF	CACF	LS	TMC
MIRFLICKR	62.81	62.33	62.42	50.25	38.02	58.44	59.95	59.13	62.51	62.45	62.00
MIRFLICKK	± 1.52	± 2.23	± 1.18	± 1.67	± 2.69	±0.93	± 1.40	± 0.27	± 1.21	± 1.39	± 1.47
NYUDv2	59.02	61.47	58.82	47.96	31.70	59.58	63.20	60.55	64.02	66.87	66.16
NTODVZ	± 4.24	± 4.05	±4.58	± 8.51	± 6.24	±3.83	±5.58	± 3.09	± 5.26	± 3.52	± 1.95
SUN-RGBD	60.28	59.43	60.83	45.22	31.61	53.52	56.97	53.53	58.14	60.78	59.00
30N-RODD	± 1.65	± 1.43	± 1.90	± 0.30	± 2.61	±2.16	± 1.11	± 0.37	± 1.94	± 2.26	± 1.99
MVSA-Single	79.83	78.36	78.29	68.40	63.39	79.32	77.78	79.51	78.03	79.25	67.50
W V SA-Shigic	± 0.87	± 2.91	± 1.31	± 7.86	± 9.19	± 0.60	± 1.05	± 1.50	± 3.56	± 2.14	± 10.49
N-MNIST+N-TIDIGITS	94.99	94.28	95.26	80.99	30.45	93.52	94.34	94.06	95.26	94.88	94.23
N-MINIST+N-TIDIOTIS	± 0.20	± 0.13	±0.13	± 1.07	± 4.91	± 0.41	± 0.77	± 0.54	± 0.27	± 0.41	± 0.34
E-MNIST+EEG	58.72	58.21	61.28	17.69	7.95	42.56	30.51	49.74	59.49	62.05	57.69
E-MNIST+EEG	± 5.12	± 1.92	±3.22	± 3.22	± 0.36	±5.66	±9.02	± 3.10	± 3.10	± 1.58	± 3.14

Table 10: Optuna hyper-parameter search space (trials = 10)

Parameter	Type	Sampler	Search Space / Candidates
lr weight_decay freeze_encoders optimtype	Continuous (log) Continuous (log) Categorical Categorical	<pre>suggest_loguniform suggest_loguniform suggest_categorical suggest_categorical</pre>	$ \begin{array}{c} [10^{-5},\ 10^{-3}] \\ [10^{-6},\ 10^{-2}] \\ \{ \texttt{True,False} \} \\ \{ \texttt{AdamW}, \texttt{RMSprop}, \texttt{Adam} \} \end{array} $

MultiOFF

Data Source and Content This datasets focus on detecting harmful content. MUTE targets troll-like behavior in image/text posts, while MultiOFF focuses on identifying offensive content and its target.

Link https://github.com/bharathichezhiyan/Multimodal-Meme-Classification-Identifying-Offensive-Content-in-Image-and-Text

Feature Extraction A ResNet is used to encode the image component, and a BERT model is used to encode the text.

Data Splits The official split is used, containing 445 training, 149 validation, and 149 test utterances.

MET-Meme (Chinese)

Data Source and Content A dataset for multimodal metaphor detection in memes, available in both English and Chinese versions.

Link https://github.com/liaolianfoka/MET-Meme-A-Multi-modal-Meme-Dataset-Rich-in-Metaphors

Feature Extraction A ResNet is used to encode the image component, and a BERT model is used to encode the text.

Data Splits We adopt an 7:1:2 split for training, validation, and test sets, containing 1,609 training, 229 validation, and 461 test utterances, with the random seed fixed at 42.

MET-Meme (English)

Data Source and Content A dataset for multimodal metaphor detection in memes, available in both English and Chinese versions.

Link https://github.com/liaolianfoka/MET-Meme-A-Multi-modal-Meme-Dataset-Rich-in-Metaphors

Feature Extraction A ResNet is used to encode the image component, and a BERT model is used to encode the text.

Data Splits We adopt an 7:1:2 split for training, validation, and test sets, containing 737 training, 105 validation, and 211 test utterances, with the random seed fixed at 42.

CH-SIMS

Data Source and Content A fine-grained single- and multi-modal sentiment analysis dataset in Chinese. It contains over 2,200 short videos with unimodal and multimodal annotations.

Link https://github.com/thuiar/MMSA

Feature Extraction We use the pre-extracted features provided by the dataset without any additional modifications.

Data Splits The official split is used, containing 1368 training, 456 validation, and 457 test utterances.

CH-SIMSv2

Data Source and Content A fine-grained single- and multi-modal sentiment analysis dataset in Chinese. It contains over 2,200 short videos with unimodal and multimodal annotations.

Link https://thuiar.github.io/sims.github.io/chsims

Feature Extraction We use the pre-extracted features provided by the dataset without any additional modifications.

Data Splits The official split is used, containing 2722 training, 647 validation, and 1034 test utterances.

Twitter2015

Data Source and Content Originating from SemEval tasks, these datasets were extended for multimodal aspect-based sentiment analysis, pairing tweets with relevant images.

Link https://archive.org/details/twitterstream

Feature Extraction A ResNet is used to encode the image component, and a BERT model is used to encode the text.

Data Splits The official split is used, containing 3179 training, 1122 validation, and 1037 test utterances.

Twitter1517

Data Source and Content

Link https://github.com/code-chendl/HFIR

Feature Extraction A ResNet is used to encode the image component, and a BERT model is used to encode the text.

Data Splits We adopt an 7:1:2 split for training, validation, and test sets, containing 3270 training, 467 validation, and 935 test utterances, with the random seed fixed at 42.

Houston2013

Data Source and Content The 2013 dataset, from the IEEE GRSS Data Fusion Contest, provides HSI and LiDAR data over the University of Houston campus, covering 15 land use classes. The 2018 version is a more complex dataset covering 20 urban land use classes.

Link https://machinelearning.ee.uh.edu/?page_id=459

Feature Extraction Following the link https://github.com/songyz2019/rs-fusion-datasets, we will proceed with the direct acquisition and loading of the dataset, which will be used for the joint classification of hyperspectral, LiDAR, and SAR data. The HSI data is processed by the conv_hsi encoder, and the LiDAR data is processed by the conv_dsm encoder.

Data Splits The official split is used, containing 2817 training and 12182 test utterances. Since the official dataset split does not include a dedicated validation set, we reuse the test set as the validation set.

Houston2018

Data Source and Content The 2013 dataset, from the IEEE GRSS Data Fusion Contest, provides HSI and LiDAR data over the University of Houston campus, covering 15 land use classes. The 2018 version is a more complex dataset covering 20 urban land use classes.

Link https://machinelearning.ee.uh.edu/2018-ieee-grss-data-fusion-challenge-fusion-of-multispectral-lidar-and-hyperspectral-data/

Feature Extraction Following the link https://github.com/songyz2019/rs-fusion-datasets, we will proceed with the direct acquisition and loading of the dataset, which will be used for the joint classification of hyperspectral, LiDAR, and SAR data. The HSI data is processed by the conv_hsi encoder, and the LiDAR data is processed by the conv_dsm encoder.

Data Splits The official split is used, containing 18750 training and 2000160 test utterances. Since the official dataset split does not include a dedicated validation set, we reuse the test set as the validation set.

MUUFL Gulfport

Data Source and Content The MUUFL dataset contains HSI and LiDAR data collected over the University of Southern Mississippi, Gulfport campus. The ground truth contains 11 urban land use classes.

Link https://github.com/GatorSense/MUUFLGulfport

Feature Extraction Following the link https://github.com/songyz2019/rs-fusion-datasets, we will proceed with the direct acquisition and loading of the dataset, which will be used for the joint classification of hyperspectral, LiDAR, and SAR data. We use the conv_hsi encoder for the HSI data and the conv_dsm encoder for the LiDAR data.

Data Splits The official split is used, containing 1100 training and 52587 test utterances. Since the official dataset split does not include a dedicated validation set, we reuse the test set as the validation set.

Trento

Data Source and Content This dataset covers a rural area south of Trento, Italy. It combines HSI data with corresponding LiDAR-derived Digital Surface Model (DSM) data, with 6 classified land cover classes.

Link https://github.com/tyust-dayu/Trento/tree/b4afc449ce5d6936ddc04fe267d86f9f35536afd

Feature Extraction Following the link https://github.com/songyz2019/rs-fusion-datasets, we will proceed with the direct acquisition and loading of the dataset, which will be used for the joint classification of hyperspectral, LiDAR, and SAR data. The HSI data is processed by conv_hsi, and the LiDAR data by conv_dsm.

Data Splits The official split is used, containing 600 training and 29614 test utterances. Since the official dataset split does not include a dedicated validation set, we reuse the test set as the validation set.

Berlin

Data Source and Content This dataset provides coregistered HSI and Synthetic Aperture Radar (SAR) data for the city of Berlin, Germany, with 8 distinct urban land cover classes.

Link https://gfzpublic.gfz-potsdam.de/pubman/faces/ ViewItemFullPage.jsp?itemId=item_1480927_5

Feature Extraction Following the link https://github.com/songyz2019/rs-fusion-datasets, we will proceed with the direct acquisition and loading of the dataset, which will be used for the joint classification of hyperspectral, LiDAR, and SAR data. The HSI data is processed by conv_hsi. The SAR data, being image-like, is processed by a ResNet encoder.

Data Splits The official split is used, containing 2820 training and 461851 test utterances. Since the official dataset split does not include a dedicated validation set, we reuse the test set as the validation set.

MDAS (Augsburg)

Data Source and Content This dataset contains multisensor data for urban area classification in Augsburg, Germany, featuring HSI and SAR imagery.

Link https://github.com/songyz2019/rs-fusion-datasets

Feature Extraction Following the link https://github.com/songyz2019/rs-fusion-datasets, we will proceed with the direct acquisition and loading of the dataset, which will be used for the joint classification of hyperspectral, LiDAR, and SAR data. The HSI data uses the conv_hsi encoder, while the SAR data is processed using a ResNet encoder.

Data Splits The official split is used, containing 761 training and 77533 test utterances. Since the official dataset split does not include a dedicated validation set, we reuse the test set as the validation set.

ForestNet

Data Source and Content A dataset for wildfire prevention, containing satellite imagery from Sentinel-2, topography data (DSM), and weather data. It's used to predict wildfire risk.

Link https://github.com/spott/ForestNet

Feature Extraction A ResNet processes satellite imagery, ResNet processes topography data, and an MLP processes tabular weather data (if needed).

Data Splits The official split is used, containing 1616 training, 473 validation, and 668 test utterances.

TCGA-BRCA

Data Source and Content Data from The Cancer Genome Atlas (TCGA) Program, focusing on Breast Cancer (BRCA). It's a multi-omics dataset, often including gene expression, DNA methylation, and copy number variation, used for tasks like survival prediction.

Link https://github.com/txWang/MOGONET

Feature Extraction Each tabular omics modality is encoded via an independent fully-connected linear layer.

Data Splits The dataset is extracted sequentially: the leading 20% forms the test set, the subsequent 5% the validation set, and the remaining 75% the training set, containing 657 training, 43 validation, and 175 test utterances.

TCGA

Data Source and Content Data from The Cancer Genome Atlas (TCGA) Program, focusing on Breast Cancer (BRCA). It's a multi-omics dataset, often including gene expression, DNA methylation, and copy number variation, used for tasks like survival prediction.

Link https://www.cancer.gov/ccg/access-data

Feature Extraction We use the TCGA dataset selected by https://github.com/bowang-lab/IntegrAO. Each tabular omics modality is encoded via an independent fully-connected linear layer.

Data Splits The dataset is extracted sequentially: the first 60% for training, the next 25% for validation, and the final 20% for testing, containing 169 training, 76 validation, and 61 test utterances.

ROSMAP

Data Source and Content Data from the Religious Orders Study and Memory and Aging Project (ROSMAP) for Alzheimer's disease research. It includes multi-omics data from post-mortem brain tissue.

Link https://github.com/txWang/MOGONET

Feature Extraction Each tabular omics modality is encoded via an independent Identity mapping encoder.

Data Splits The dataset is extracted sequentially: the first 60% for training, the next 25% for validation, and the final 20% for testing, containing 194 training, 87 validation, and 70 test utterances.

SIIM-ISIC

Data Source and Content From the 2020 SIIM-ISIC Melanoma Classification Kaggle challenge. The dataset contains thousands of dermoscopic images of skin lesions, with patient-level metadata, for classifying lesions.

Link https://www.kaggle.com/competitions/siim-isic-melanoma-classification/data

Feature Extraction A ResNet encoder is used for the dermoscopic images, and an independent Identity mapping encoder is used for the tabular patient metadata.

Data Splits We adopt an 8:1:1 split for training, validation, and test sets, containing 26502 training, 3312 validation, and 3312 test utterances, with the random seed fixed at 42.

Derm7pt

Data Source and Content A multiclass skin lesion classification dataset based on the 7-point checklist. It provides dermoscopic images and a corresponding vector of semi-quantitative clinical features.

Link https://www.kaggle.com/datasets/menakamohanakumar/derm7pt

Feature Extraction The images are encoded with a CN-NEncoder, while the tabular clinical feature vectors are encoded with Identity mapping encoder.

Data Splits The official split is used, containing 413 training, 203 validation, and 395 test utterances.

GAMMA

Data Source and Content From the Glaucoma grAding from Multi-Modality imAges challenge. It contains color fundus images and stereo-pairs of disc photos for glaucoma diagnosis.

Link https://zenodo.org/records/15119049

Feature Extraction Both the fundus images and stereopair images are encoded using a CNNEncoder.

Data Splits The dataset is extracted sequentially: the first 20% for training, the next 10% for validation, and the final 70% for testing, containing 20 training, 10 validation, and 70 test utterances.

MIMIC-III

Data Source and Content A large, de-identified ICU database containing structured data (lab results, vitals) and unstructured clinical notes for over 40,000 patients. It's used for tasks like mortality prediction.

Link https://physionet.org/content/mimiciii/1.4/

Feature Extraction Modality is encoded by a Time-SeriesTransformerEncoder and Identity mapping.

Data Splits The dataset is extracted sequentially: the leading 20% forms the test set, the subsequent 5% the validation set, and the remaining 75% the training set, containing 24462 training, 1631 validation, and 6523 test utterances.

MIMIC-CXR

Data Source and Content A large-scale dataset containing over 377,000 chest X-ray images and their corresponding free-text radiology reports.

Link https://physionet.org/content/mimic-cxr-jpg/2.1.0/

Feature Extraction We use a ResNet encoder for the chest X-ray images and a BERT model for the radiology reports.

Data Splits Following the official split, we cap the training set to a maximum of 5,000 utterances, yielding 5,000 for training, 2942 for validation, and 5117 for test. We set the random seed=42 to select the training samples.

eICU

Data Source and Content A multi-center ICU database with de-identified data for over 200,000 admissions from hospitals across the US. It contains high-granularity vital sign data and clinical notes.

Link https://eicu-crd.mit.edu/https://physionet.org/content/eicu-crd/2.0/

Feature Extraction All modalities are encoded using the identity mapping.

Data Splits The corpus is hierarchically partitioned: an initial 80 / 20 split isolates the test set; the remaining 80% is then subdivided at a 15 : 1 ratio, producing final allocations of approximately 75% training, 5% validation, and 20% test. We then get 5727 training, 382 validation, and 1528 test utterances. The random seed is fixed at 42.

MIRFLICKR

Data Source and Content A dataset of one million images from the Flickr website with their associated user-assigned tags. A 25,000-image subset with curated labels is commonly used for multimodal retrieval and classification.

Link https://press.liacs.nl/mirflickr/

Feature Extraction A ResNet is used for the images, and a BERT model is used for the textual tags.

Data Splits We adopt an 7:1:2 split for training, validation, and test sets, containing 14010 training, 2001 validation, and 4004 test utterances, with the random seed fixed at 42.

CUB Image-Caption

Data Source and Content An extension of the Caltech-UCSD Birds-200-2011 dataset. It pairs detailed bird images with rich, descriptive text captions, ideal for fine-grained image-text matching.

Link https://github.com/iffsid/mmvae

Feature Extraction The bird images are encoded with a ResNet, and the text captions are encoded with a BERT model.

Data Splits We adopt an 7:1.5:1.5 split for training, validation, and test sets, containing 82510 training, 17680 validation, and 17690 test utterances, with the random seed fixed at 2025.

SUN-RGBD

Data Source and Content A large-scale dataset for indoor scene understanding. It contains over 10,000 RGB-D (color and depth) images with dense annotations.

Link https://rgbd.cs.princeton.edu/

Feature Extraction We use a ResNet encoder for the RGB images and a similar ResNet architecture for the depth maps.

Data Splits The official split is used, containing 4845 training and 4659 test utterances. Since the official dataset split does not include a dedicated validation set, we reuse the test set as the validation set.

NYUDv2

Data Source and Content The NYU-Depth Dataset V2 provides RGB and Depth images of various indoor scenes captured from a Microsoft Kinect, with dense labels for semantic segmentation.

Link https://cs.nyu.edu/~fergus/datasets/nyu_depth_v2. html

Feature Extraction A ResNet encoder is used for the RGB images and another for the depth images.

Data Splits The official split is used, containing 795 training, 414 validation, and 654 test utterances.

UPMC-Food101

Data Source and Content An extension of Food-101, this dataset pairs food images with their ingredient lists for tasks like recipe retrieval from images.

Link https://www.kaggle.com/datasets/gianmarco96/upmcfood101

Feature Extraction We follow https://github.com/facebookresearch/mmbt to prepare the splits. A ResNet encodes the food images, while a BERT model encodes the ingredient lists.

Data Splits The official split is used, containing 62971 training, 5000 validation, and 22715 test utterances.

MVSA-Single

Data Source and Content A Multi-View Sentiment Analysis dataset containing image-text posts from Twitter. The "Single" variant contains posts where the sentiment label is consistent across annotators.

Link https://www.kaggle.com/datasets/vincemarcs/mvsasingle

Feature Extraction We follow https://github.com/facebookresearch/mmbt to prepare the splits. Images are encoded using ResNet, and the tweet text is encoded using BERT.

Data Splits The official split is used, containing 1555 training, 518 validation, and 519 test utterances.

MNIST-SVHN

Data Source and Content This is a synthetic dataset combining two famous digit recognition datasets: MNIST (handwritten digits) and SVHN (street view house numbers). The task is to classify pairs of digits.

Link https://github.com/iffsid/mmvae

Feature Extraction We apply a flattening operation to MNIST images, whereas SVHN images are processed by a simple CNN encoder.

Data Splits The official split is used, containing 560,680 training and 100,000 test utterances. Since the official dataset split does not include a dedicated validation set, we reuse the test set as the validation set.

N-MNIST+N-TIDIGITS

Data Source and Content Neuromorphic versions of MNIST (vision) and TIDIGITS (audio-spoken digits). Data is recorded as asynchronous event streams (spikes) from event-based sensors.

Feature Extraction We follow https://github.com/MrLinNing/MemristorLSM, and pair each N-MNIST frame with its corresponding N-TIDIGITS audio clip to form unique image—sound pairs and perform classification on these aligned inputs. NMNIST frames are encoded by a CNN; NTIDIGITS MFCCs are encoded by an LSTM.

Data Splits The dataset is extracted sequentially: the first 70% for training, the next 15% for validation, and the final 15% for testing, containing 2835 training, 603 validation, and 612 test utterances.

E-MNIST+EEG

Data Source and Content A dataset that combines images from the E-MNIST dataset (handwritten letters/digits) with simultaneously recorded EEG brain signals from subjects viewing them.

Feature Extraction We follow https://github.com/MrLinNing/MemristorLSM, and construct unique image–EEG pairs by pairing each E-MNIST sample with its corresponding EEG recording, and then perform classification on these paired inputs. The E-MNIST images are encoded with a CNN, and the time-series EEG signals are encoded with an LSTM encoder.

Data Splits The dataset is extracted sequentially: the first 70% for training, the next 15% for validation, and the final 15% for testing, containing 468 training, 104 validation, and 130 test utterances.